Journal of Hazardous Materials 170 (2009) 639–644

Contents lists available at ScienceDirect

Journal of Hazardous Materials

journal homepage: www.elsevier.com/locate/jhazmat

Synthesis of zeolite Li-ABW from fly ash by fusion method

Z.T. Yao, M.S. Xia, Y. Ye*, L. Zhang

Department of Earth Science, College of Science, Zhejiang University, Hangzhou 310027, PR China

ARTICLE INFO

Article history:
Received 23 March 2009
Received in revised form 5 May 2009
Accepted 5 May 2009
Available online 18 May 2009

Keywords:
Zeolite Li-ABW
Fly ash
Fusion method
Lithium hydroxide monohydrate

ABSTRACT

The zeolite Li-ABW was synthesized by fusion method using fly ash as raw material. It comprised alkaline fusion followed by hydrothermal treatment in $LiOH{\cdot}H_2O$ medium. Crystallinity of zeolite as high as 97.8% was attained under the following conditions: $LiOH{\cdot}H_2O$ concentration, 3 M; hydrothermal temperature, 180 °C; the corresponding aging time, 12 h. The content of Li-ABW increased at the expense of lithium aluminum silicate or quartz with an increase of $LiOH{\cdot}H_2O$ concentration. With increasing hydrothermal temperature and aging time, the soluble species re-crystallized and crystalline phase transformation between different zeolites was observed. Scanning electron microscopy (SEM) observation revealed that the obtained zeolite Li-ABW was a rod-like crystal. The pore size distribution curve indicated the presence of mesopores.

© 2009 Elsevier B.V. All rights reserved.

1. Introduction

Fly ash is a by-product derived from burning of coal during the generation of electricity in thermal power plant. More than 600 million tons of fly ash is produced annually in the world [1,2]. This waste must be reduced prior to disposal. Recently, the recycle of fly ash are tried to proceed aggressively. For example, about 20% fly ash has been used to replace a portion of cement in concrete production due to its pozzolanic and cementitious properties. It has also been used in road base construction, soil amendment, sewage sludge treatment and as filler in plastic composite materials [2,3]. However, the utilization rate for fly ash in these applications is far less than that of the ash being generated. More than half of it finds no applications and is discharged into ash ponds or landfills. In the future, lacking of landfill space and escalating disposal costs are anticipated, so new recycle technologies for fly ash are desired to develop [4].

Synthesis of zeolite products is noticed as one of the effective usages for fly ash [5,6]. It is possible due to its high content of amorphous aluminosilicate glass (about 80%) [7] and the high specific surface area. Zeolite was firstly synthesized from fly ash by Holler and Wirsching in 1985 [8]. Since then, many different types of zeolites, such as zeolite X [9,10], zeolite ZSM-5 [11], zeolite Na-P1 [12,13] and zeolite A [14–16] are synthesized by applying many synthesis methods.

Zeolite Li-ABW ($LiAlSiO_4{\cdot}H_2O$) is a synthetic low silica zeolite, which possesses the ABW framework topology. It was first synthesized by Barrer and White in 1951 [17] and usually using Na-LTA with lithium chloride as precursors [18,19]. However, there is no report on the synthesis of zeolite Li-ABW using fly ash as raw material by fusion method. The fusion method was suggested by Shigemoto and Hayashi [20]. It includes an alkaline fusion stage prior to the conventional hydrothermal process, which could significantly improve the zeolitization process. Thus, in the present study, we attempt to synthesize zeolite Li-ABW from fly ash by hydrothermal treatment after fusion pretreatment with $LiOH{\cdot}H_2O$. The influences of reaction conditions, such as $LiOH{\cdot}H_2O$ concentration, hydrothermal temperature and aging time on the products were investigated to optimize the synthesis. The obtained zeolite were also characterized and analyzed by means of Fourier transform IR spectroscopy (FTIR), differential thermal analysis (TG-DTA) and N_2 adsorption isotherms.

2. Experimental

2.1. Materials

The fly ash sample used in this study was obtained from Hangzhou thermal power plant in China. The chemical compositions were determined by X-ray fluorescence (XRF, Shimadzu XRF-1800) and the results were as follows (wt.%): SiO_2 50.5, Al_2O_3 35.9, Fe_2O_3 5.3, CaO 4.6, TiO_2 1.5, K_2O 1.3 and others 0.9. Fig. 1 indicates that the main crystalline phases in fly ash sample are mullite (JCPDS card no. 15-776) and quartz (JCPDS card no. 5-490) together with amorphous component by X-ray diffraction (XRD) analysis.

2.2. Pretreatment of fly ash sample

The magnetite content in fly ash influences the properties of zeolites [20]. As magnetic separation is an effective approach for iron

* Corresponding author. Tel.: +86 571 87953217; fax: +86 571 87951336.
E-mail address: gsyeying@zju.edu.cn (Y. Ye).

0304-3894/$ – see front matter © 2009 Elsevier B.V. All rights reserved.
doi:10.1016/j.jhazmat.2009.05.018

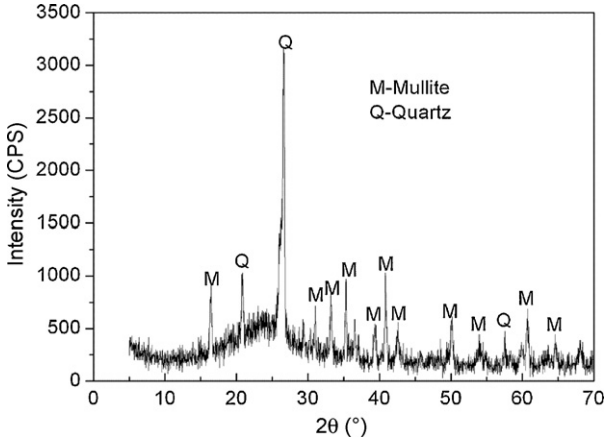

Fig. 1. XRD pattern of the fly ash.

removal, it was used in this work. The magnetic separation was performed on WCF-2 multi-purpose magnetic analytical meter (Beijing Geological Instrument Factory) with a constant magnetic current of 2.8 A. The content of iron components in ash after pretreatment was also determined. The result showed that it was reduced significantly from 5.3% to 0.69%.

2.3. Synthesis process

The fusion method comprises two stages [20]. Typical alkaline fusion and the succeeding hydrothermal treatment were carried out as follows.

2.3.1. Alkaline fusion process

The magnetically pretreated fly ash was mixed and ground with 25% $LiOH{\cdot}H_2O$ to obtain a homogeneous mixture. Then, the mixture was heated in a ceramic crucible in air at 980 °C for 1 h.

2.3.2. Alkaline hydrothermal process

The resultant fused mixture was cooled to room temperature, ground again and dissolved in $LiOH{\cdot}H_2O$ solutions with S/L ratio of 1:2. Different $LiOH{\cdot}H_2O$ concentrations (1.0, 1.5, 2.0, 2.5 and 3.0 M) were used to explore the influence on products. Then, the mixture was put into autoclave made of stainless steel and a hydrothermal treatment was conducted. The reaction temperature and time were set at a desired temperature (80, 100, 120, 160 and 180 °C) for a given period (12 h, unless otherwise stated). In order to discover the crystalline phases and morphology of the products as a function of time, different aging time (2, 6, 8, 10, 12 and 16 h) was used. At the end of the process, the solid is separated by filtration, washed repeatedly with distilled water and then dried at overnight at 100 °C.

2.4. Characterization

The products thus obtained were characterized by various conventional methods. The XRD analysis was employed to determine the crystalline phases. A Rigaku D-Max/IIB X-ray power diffractometer operated at 40 kV and 30 mA, with Cu Kα as the radiation source. The detector was scanned at a step scan of 0.02° and a scan speed of 4°/min. The relative crystallinity R_I of zeolite was calculated according to following formula: $R_I = D_{I,sample}/D_{I,reference}$. Scanning electron microscopy (SEM) investigations were conducted in a Hitachi S-4800 scanning electron microscope to observe the microstructure of the samples. Transmission IR spectra was recorded by a Nicolet Nexus-670 Fourier transform infrared (FTIR) spectrometer with a resolution of 2 cm^{-1} using a KBr disc method. The thermal behavior of obtained zeolite was observed through

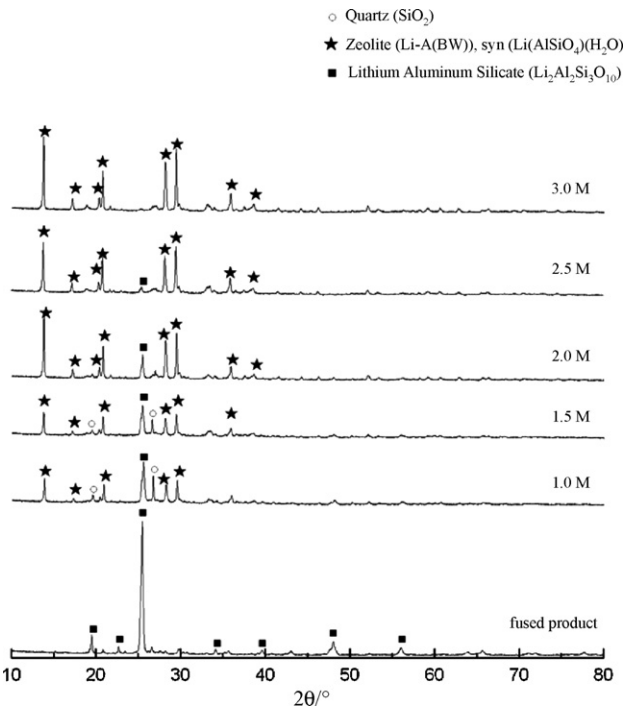

Fig. 2. XRD patterns of the products in hydrothermal process with different alkaline concentrations (synthesis conditions: hydrothermal temperature 180 °C, aging time 12 h).

TG-DTA analysis and conducted by a ZRY-2P simultaneous thermal analyzer (Precision & Science Instrument Co. Ltd., Shanghai, China). The sample was heated in air from ambient temperature to 1000 °C at a fixed heating rate of 10 °C/min. The N_2 adsorption measurement was carried out to evaluate the specific surface area and pore volume of the zeolite. Nitrogen adsorption–desorption isotherms were recorded at 77 K using a Micromeritics model ASAP 2020 adsorption analyzer. The pore size distribution was evaluated from the desorption branch of isotherm using Barret–Joyner–Halenda (BJH) method.

3. Results and discussion

3.1. Influence of the $LiOH{\cdot}H_2O$ concentration

A series of experiments were undertaken to determine the influence of $LiOH{\cdot}H_2O$ concentration on products. For a comparison, the XRD pattern of fused fly ash before hydrothermal treatment has also been included in Fig. 2. It was found that the main crystalline phase of fused product is lithium aluminum silicate ($Li_2Al_2Si_3O_{10}$, JPCDS card no. 25-1183). In the hydrothermal process, the fused products were gradually dissolved and conversed into zeolites. When the $LiOH{\cdot}H_2O$ concentrations are less than 2.0 M, the main phases are zeolite Li-ABW (JPCDS card no. 73-1498) with little quartz (SiO_2, JPCDS card no. 79-1910) and lithium aluminum silicate detected. It indicated a lower degree of zeolitization. The $LiOH{\cdot}H_2O$ concentration is low in the thermal system with a result of quartz and lithium aluminum silicate being not well dissolved. Further increases in the proportion of $LiOH{\cdot}H_2O$ in the system resulted in the intensity of zeolite Li-ABW reflections increasing at the expense of lithium aluminum silicate. It is clear that controlling alkaline concentration is very important to maintain purity of the zeolite. The results indicated that the preferred $LiOH{\cdot}H_2O$ concentration in hydrothermal process was 3.0 M. The concentration was selected for further studies.

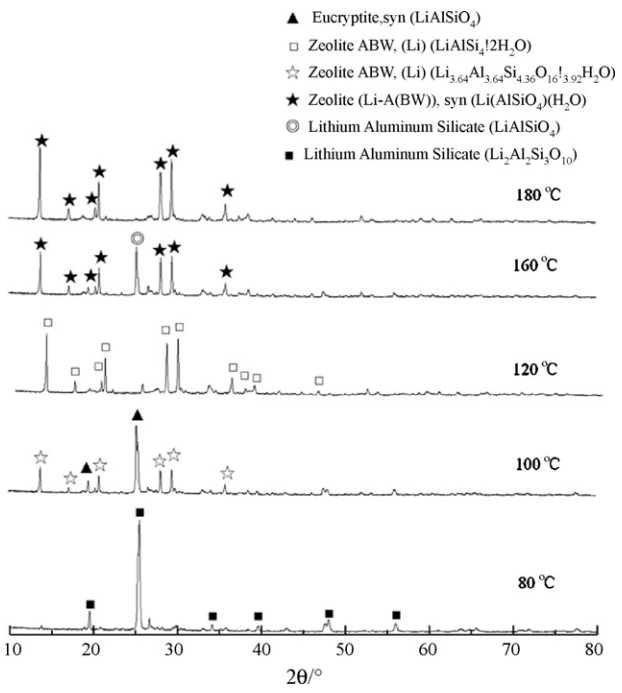

Fig. 3. XRD patterns of the products in hydrothermal process at different temperature (synthesis conditions: alkaline concentration 3.0 M, aging time 12 h).

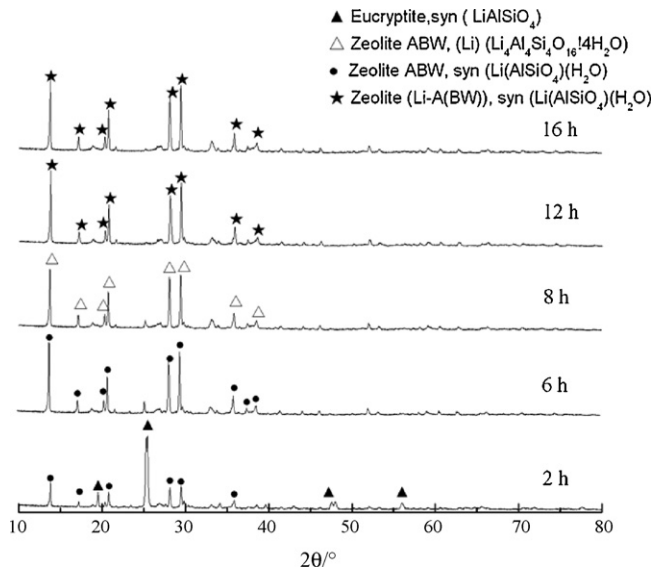

Fig. 4. XRD patterns of the products in hydrothermal process with different aging time (synthesis conditions: alkaline concentration 3.0 M, hydrothermal temperature 180 °C).

3.2. Influence of the hydrothermal temperature

The influence of varying hydrothermal temperature is plotted in Fig. 3. It was clear that there existed no notably modification for fused product after treatment at 80 °C. It indicated that the temperature 80 °C did not provide enough activation. With an increase of temperature up to 100 °C, the eucryptite ($LiAlSiO_4$, JPCDS card no. 75-2330) and zeolite ABW phase ($Li_{3.64}Al_{3.64}Si_{4.36}O_{16}{\cdot}3.92H_2O$, JPCDS card no. 39-215) were observed, indicating the fused product started being dissolved and promoted the crystal growth. At 120 °C, the dissolved silicon and aluminium favored the formation of zeolite ABW ($LiAlSiO_4{\cdot}2H_2O$, JPCDS card no. 27-1211). Whereas at 160 °C, the product was conformed by a mix of zeolite Li-ABW and lithium aluminum silicate ($LiAlSiO_4$, JPCDS card no. 26-840). The phase transformation was possible because that the zeolite ABW was not stable and later re-dissolved or re-crystallized. Further increase in the hydrothermal temperature, the soluble species completely conversed into zeolite Li-ABW, showing the onset temperature of zeolite Li-ABW forming was 180 °C.

3.3. Influence of the aging time

Fig. 4 illustrates the evolution of zeolite synthesis as a function of time in thermal process. The main phases of product after crystallization for 2 h are eucryptite and zeolite ABW ($LiAlSiO_4{\cdot}H_2O$, JPCDS card no. 80-463). When the time prolonged from 6 to 12 h, zeolite ABW ($LiAlSiO_4{\cdot}H_2O$), zeolite ABW ($Li_4Al_4Si_4O_{16}{\cdot}4H_2O$, JPCDS card no. 41-554) and zeolite Li-ABW were detected, respectively. This transformation coincided with Ostwald's rule of successive transformation [15]. With the rise of aging time, the increase in supersaturation achieved as a result of the higher proportion of soluble species. The higher the supersaturation, the better the conditions to nucleate metastable phases [21], such as zeolite ABW, which later re-dissolved or re-crystallized and were replaced by a more stable zeolite Li-ABW. All diffraction peaks for product after aging for 12 h was perfectly indexed to zeolite Li-ABW. The crystallinity reached as high as 97.8%. No peaks due to other phases were detected, indicating the high purity of zeolite. The XRD pattern for product after 16 h showed no significant difference, indicating the successive transformation completed. These results indicated that the optimal aging time was 12 h.

SEM investigations are conducted to explore the morphology evolution of the samples. For a comparison, SEM images of the fly ash before and after alkaline fusion have also been included in Fig. 5. The fly ash sample was characterized by spherically and irregularly round-shaped, a typical particle morphology for fly ash. After fusion treatment, the agglomeration is observed. The particles were substantially interlocked together and reduced in size. SEM observation showed that the surface of the fused product became rough, indicating the fly ash was activated. At a crystallization time of 2 h, the product manifested as a rod-like crystal with average 6 μm in length, binding of irregular particles. The rod-like crystal was observed to become prominent and increased in length after aging for 6 h. Thereafter, the morphology showed no significant change when the time prolonged up to 8 h. This was evidenced by the XRD analysis (Fig. 4), which showed that the products crystallized for 6 and 8 h were both zeolite ABW, although their chemical formula was not exactly the same. The zeolite Li-ABW was confirmed forming at a crystallization time of 12 h. We observed its morphology by SEM and it was a rod-like crystal, which was in accordance with the literature [22]. The morphology of product after 16 h was no significant change and was not included in Fig. 5.

It is worth mentioning that the morphology of zeolite Li-ABW differed from the irregular round-shaped morphology for fused product, which indicated that the fused product was completely dissolved and then re-crystallized. However, the conditions in the conventional hydrothermal process give difficulties in the dissolution of quartz and mullite, so the resultant product varies widely and usually co-crystallized of zeolites with original crystalline phases (quartz and mullite). The zeolite zone was formed like an egg white, covering the central core of fly ash particles [10]. Therefore, in addition to using a longer aging period, adding Na_2SiO_3 or $NaAlO_2$ powder to modify Si/Al ratio was also conducted in order to achieve the highest level of zeolitization. It is generally known that the formation of particular zeolite species depends greatly upon the Si/A1 ratio in the starting material for hydrothermal reaction [21]. In the present work, there was no modification of Si/Al molar ratio to the fly ash. It was because that the Si/Al molar ratio in fly ash sample was 1.2 compared with that of 1.0 in zeolite Li-ABW. In

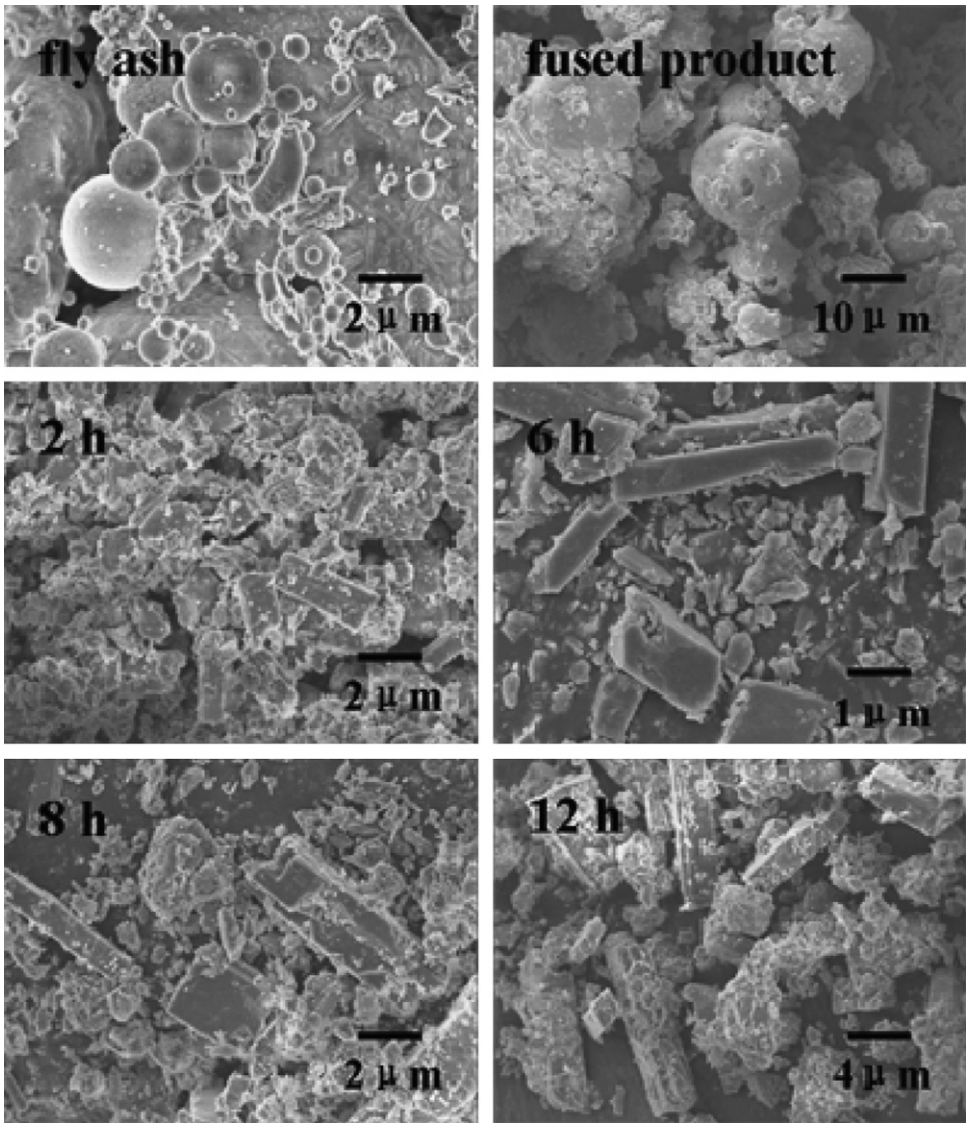

Fig. 5. SEM images of the products in hydrothermal process with different aging time (synthesis conditions: alkaline concentration 3.0 M, hydrothermal temperature 180 °C).

the hydrothermal process, the fused product riched in Si and Al was completely dissolved and selectively conversed into zeolite Li-ABW. This transform automatically proceed according to the demand of Si/Al ratio for zeolite species. In this study, the content of Si was a little more than that of Al, so the residue of Si was left in solution. Although the synthesis was at the expense of little Si loss, the yield of zeolite was as high as 78.9%. But in the succeeding planning study, it may be advisable to add Na_2SiO_3 or $NaAlO_2$ meeting the demand of Si/Al molar ratio for desired zeolite and promoting the zeolite yield. The other is worthy noting that the zeolite Li-ABW was synthesized by fusion method with hydrothermal process at 180 °C for 12 h. The aging time was significantly shorter as compare with 6 d and 72 h in the literatures [18,19]. Although the hydrothermal temperature 180 °C was also lower than that in the literatures as 220 and 250 °C [18,19], the fusion process was at quite high temperature (980 °C).

3.4. FTIR spectrum

The fly ash sample was subjected to alkaline fusion and then experienced hydrothermal reaction in 3 M $LiOH{\cdot}H_2O$ solution at 180 °C for 12 h. Thereafter, the zeolite Li-ABW was obtained. Its FTIR transmittance spectrum is presented in Fig. 6. The significant broad peaks were located at approximately 3473 and 1637 cm^{-1} for O–H stretching and bending, respectively. The band 1087–939 cm^{-1} was assigned to the asymmetric stretching vibration of Si–O–Si

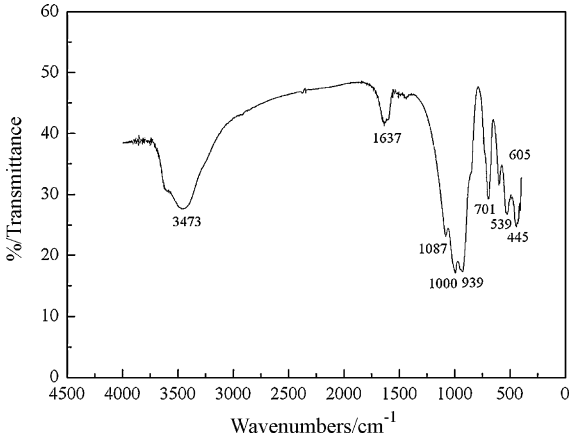

Fig. 6. FTIR spectrum of the zeolite Li-ABW.

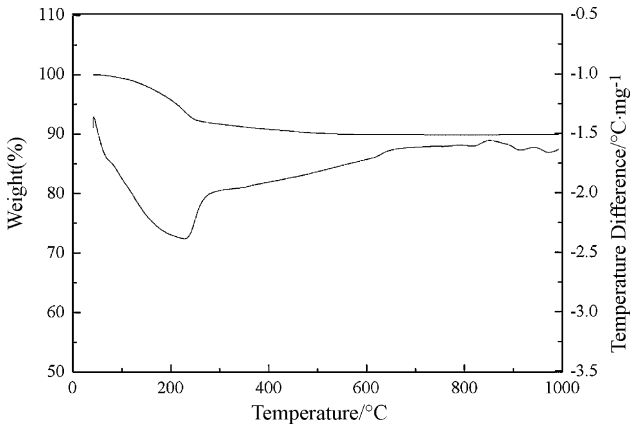

Fig. 7. TG-DTA curves of the zeolite Li-ABW.

bond within [SiO_4] [23,24]. The band 701–605 cm^{-1} was known to belong to Si–O–Si symmetric stretching vibration. While, the band 445–539 cm^{-1} was due to bending vibration of Si–O–Si and Si–O–Al linkage [25,26].

3.5. TG-DTA results

TG-DTA studies of the zeolite Li-ABW are displayed in Fig. 7. It indicated a two-stage mass loss. At the first stage, ca. 7.96% loss was occurred at about 250 °C accompanied by an endothermal peak. This was reasonable due to the loss of the adsorbed and occluded water molecules in zeolite crystal. The second occurred continuously between 250 and 850 °C with a small mass loss of 2.14%. The loss was not accompanied by significant exothermal or endothermal peaks. These results indicated the remarkable thermal stability of zeolite Li-ABW.

3.6. N_2 adsorption surface area and pore size distribution

Fig. 8 illustrates the N_2 adsorption-desorption plots at 77 K for zeolite Li-ABW. The pattern corresponded to the type IV of the BDDT classification. Moreover, desorption branch corresponded to the H1 type of the IUPAC classification [27]. There was a steep increase in the amount of nitrogen adsorbed when the relative pressure (P/P_0) was higher than 0.8. The existence of a hysteresis loop in the isotherms indicated the presence of mesopores, whereas the shape of the hysteresis loop was related to the shape of the mesopores [28,29]. Roughly, the vertical hysteresis loop indicated cylindrical mesopores. H1 type isotherm is associated to narrow pore size distribution. It was evidenced in Fig. 8 (inset), whereby the sample showed a monomodal pore average size distribution with maximum value 32.03 Å.

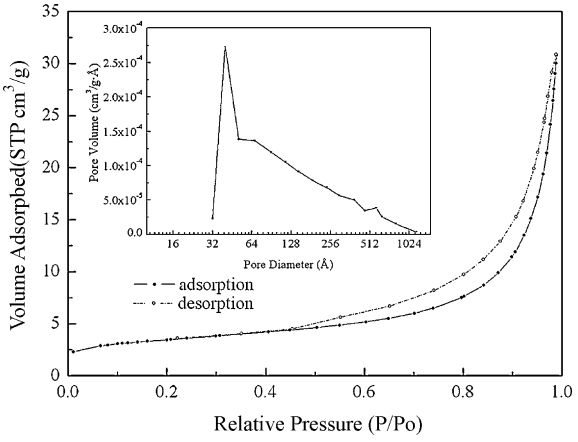

Fig. 8. Nitrogen adsorption-desorption isotherms of the zeolite Li-ABW and corresponding pore diameter distribution pattern (inset).

4. Conclusions

From the experimental results the following conclusions can be drawn:

1) The optimal conditions for fused product were identified as being crystallized in 3 M $LiOH{\cdot}H_2O$ medium and incubated at 180 °C for 12 h.
2) SEM observation revealed that the zeolite Li-ABW was a rod-like crystal. TG-DTA results indicated that it had remarkable thermal stability. The pore size distribution curve showed the presence of mesopores.

Acknowledgments

We gratefully acknowledge financial support from Chinese National 863 High Technology (Grant no. 2007AA06Z128). The authors gratefully acknowledge Dr. Jipeng Cheng (Zhejiang University, Hangzhou, China) for recording the SEM images.

References

[1] C.F. Wang, J.S. Li, L.J. Wang, X.Y. Sun, Influence of NaOH concentrations on synthesis of pure-form zeolite A from fly ash using two-stage method, J. Hazard. Mater. 155 (2008) 58–64.
[2] H. Cho, D. Oh, K. Kim, A study on removal characteristics of heavy metals from aqueous solution by fly ash, J. Hazard. Mater. B 127 (2005) 187–195.
[3] M. Ilic, C. Cheeseman, C. Sollars, J. Knight, Mineralogy and microstructure of sintered lignite coal fly ash, Fuel 82 (2003) 331–336.
[4] F.K. Nihon, K. Kankyogijyutsu, Coal Ash Handbook, 4th edition, Tokyo, 2005.
[5] N. Shigemoto, H. Hayashi, K. Miyaura, Selective formation of Na-X, zeolite from coal fly ash by fusion with sodium hydroxide prior to hydrothermal reaction, J. Mater. Sci. 28 (1993) 4781–4786.
[6] C.F. Lin, H.C. His, Resource recovery of waste fly ash: synthesis of zeolite-like materials, Environ. Sci. Technol. 29 (1995) 1109–1117.
[7] G. Steenbruggen, G.G. Hollman, The synthesis of zeolites from fly ash and the properties of the zeolite products, J. Geochem. Explor. 62 (1998) 305–309.
[8] H. Holler, U. Wirsching, Zeolite formation from fly ash, Forsch. Miner. 63 (1985) 21–43.
[9] H. Tanaka, Y. Sakai, R. Hino, Formation of Na-A and Na-X zeolites from waste solutions in conversion of coal fly ash to zeolites, Mater. Res. Bull. 37 (2002) 1873–1884.
[10] N. Shigemoto, H. Hayshi, Selective formation of Na-X zeolite from coal fly ash by fusion with sodium prior to hydrothermal reaction, J. Mater. Sci. 28 (1993) 4781–4786.
[11] M. Chareonpanich, T. Namto, P. Kongkachuichay, J. Limtrakul, Synthesis of ZSM-5 zeolite from lignite fly ash and rice husk ash, Fuel Process. Technol. 85 (2004) 1623–1634.
[12] M. Inada, Y. Eguchi, N. Enomoto, J. Hojo, Synthesis of zeolite from coal fly ashes with different silica-alumina composition, Fuel 84 (2005) 299–304.
[13] M. Inada, H. Tsujimoto, Y. Eguchi, N. Enomo, J. Hojo, Microwave-assisted zeolite synthesis from coal fly ash in hydrothermal process, Fuel 84 (2005) 1482–1486.
[14] K.S. Hui, C.Y.H. Chao, Effects of step-change of synthesis temperature on synthesis of zeolite 4A from coal fly ash, Mesoporous Mater. 88 (2006) 145–151.
[15] S.S. Rayalu, J.S. Udhoji, K.N. Munshi, M.Z. Hasan, Highly crystalline zeolite-A from fly ash of bituminous and lignite coal combustion, J. Hazard. Mater. 88 (2001) 107–201.
[16] K.S. Hui, C.Y.H. Chao, Pure, single phase, high crystalline, chamfered-edge zeolite 4A synthesized from coal fly ash for use as a builder in detergents, J. Hazard. Mater. B 137 (2006) 401–409.
[17] R.M. Barrer, E.A. White, The hydrothermal chemistry of silicates. Part I. Synthetic lithium aluminosilicates, J. Chem. Soc. (1951) 1267–1278.
[18] J.X. Dong, X.Y. Wang, H. Xu, Q. Zhao, J.P. Li, Hydrogen storage in several microporous zeolites, Int. J. Hydrogen Energy 32 (2007) 4998–5004.
[19] H. Robson, Verified Syntheses of Zeolitic Materials, 2nd edition, Elsevier, Amsterdam, 2001.
[20] A. Molina, C. Poole, A comparative study using two methods to produce zeolite from fly ash, Miner. Eng. 17 (2004) 167–173.
[21] R.M. Barrer, Hydrothermal Chemistry of Zeolites, Academic Press, London, 1982.
[22] D.C. Lin, X.W. Xu, F. Zuo, Y.C. Long, Crystallization of JBW, CAN, SOD and ABW type zeolite from transformation of meta-kaolin, Microporous Mesoporous Mater. 70 (2004) 63–70.

[23] G. Lusvardi, G. Malavasi, L. Menabue, M.C. Menziani, A. Pedone, U. Segre, A computational tool for the prediction of crystalline phases obtained from controlled crystallization of glasses, J. Phys. Chem. B 109 (2005) 21586–21592.
[24] P. Pisciella, M. Pelino, Thermal expansion investigation of iron rich glass-ceramic, J. Eur. Ceram. Soc. 28 (2008) 3021–3026.
[25] M.S. Ma, W. Ni, Y.L. Wang, Z.J. Wang, F.M. Liu, The effect of TiO_2 on phase separation and crystallization of glass-ceramics in CaO-MgO-Al_2O_3-SiO_2-Na_2O system, J. Non-Cryst. Solids. 354 (2008) 5395–5401.
[26] H. Rawson, Inorganic Glass-Forming Systems, Academic Press, London and New York, 1967.
[27] S.J. Gregg, K.S.W. Sing, Adsorption Surface Area and Porosity, Academic Press, London, 1991.
[28] S. Morin, P. Ayrault, N.S. Gnep, M. Guisnet, Influence of the framework composition of commerical HFAU zeolites on their activity and selectivity in *m*-xylene transformation, Appl. Catal. A: Gen. 166 (1998) 281–292.
[29] A.H. Janssen, A.J. Koster, K.P. de Jong, On the shape of the mesoporous in zeolite Y: a three-dimensional transmission electron microscopy study combined with texture analysis, J. Phys. Chem. B 106 (2002) 11905–11909.